The Utility of X-Band Polarimetric Radar for Quantitative Estimates of Rainfall Parameters

SERGEY Y. MATROSOV, DAVID E. KINGSMILL, AND BROOKS E. MARTNER

Cooperative Institute for Research in Environmental Sciences, University of Colorado, and NOAA/Environmental Technology Laboratory, Boulder, Colorado

F. MARTIN RALPH

NOAA/Environmental Technology Laboratory, Boulder, Colorado

(Manuscript received 17 August 2004, in final form 22 December 2004)

ABSTRACT

The utility of X-band polarimetric radar for quantitative retrievals of rainfall parameters is analyzed using observations collected along the U.S. west coast near the mouth of the Russian River during the Hydrometeorological Testbed project conducted by NOAA's Environmental Technology and National Severe Storms Laboratories in December 2003 through March 2004. It is demonstrated that the rain attenuation effects in measurements of reflectivity (Z_e) and differential attenuation effects in measurements of differential reflectivity (Z_{DR}) can be efficiently corrected in near–real time using differential phase shift data. A scheme for correcting gaseous attenuation effects that are important at longer ranges is introduced. The use of polarimetric rainfall estimators that utilize specific differential phase and differential reflectivity data often provides results that are superior to estimators that use fixed reflectivity-based relations, even if these relations were derived from the ensemble of drop size distributions collected in a given geographical region. Comparisons of polarimetrically derived rainfall accumulations with data from the high-resolution rain gauges located along the coast indicated deviation between radar and gauge estimates of about 25%. The Z_{DR} measurements corrected for differential attenuation were also used to retrieve median raindrop sizes, D_0. Because of uncertainties in differential reflectivity measurements, these retrievals are typically performed only for $D_0 > 0.75$ mm. The D_0 estimates from an impact disdrometer located at 25 km from the radar were in good agreement with the radar retrievals. The experience of operating the transportable polarimetric X-band radar in the coastal area that does not have good coverage by the National Weather Service radar network showed the value of such radar in filling the gaps in the network coverage. The NOAA X-band radar was effective in covering an area up to 40–50 km in radius offshore adjacent to a region that is prone to flooding during wintertime landfalling Pacific storms.

1. Introduction

Meteorological radars that operate at X band ($\lambda \sim 3$ cm) have been traditionally limited in their applicability for quantitative precipitation estimations (QPEs) due to a relatively high attenuation rate of radar signals in rain. However, the use of polarimetric approaches provides a new tool for correcting attenuation effects, thus greatly increasing the utility of X-band radars for QPE. With attenuation correction issues properly addressed, some advantages of X-band radars over longer-wavelength radars operating at C ($\lambda \sim 5$ cm) or S band ($\lambda \sim 10$ cm) become evident. These advantages include higher mobility, smaller size and cost, lower power requirements, potentially higher spatial resolution and stronger differential phase signals. All these traits are important for the prospective radar systems designed to complement the National Weather Service (NWS) operational radar network of Weather Surveillance Radar-1988 Doppler [WSR-88D; Next-Generation Weather Radar (NEXRAD)] by filling important gaps in NEXRAD coverage (National Research Council 2004).

A number of polarimetric transportable X-band radars have been introduced for QPE studies in the last few years (e.g., Matrosov et al. 1999; Iwanami et al. 2001; Wurman 2001). Initial tests and validations of X-band radar QPE results were performed during several field campaigns (e.g., Matrosov et al. 2002; Anagnostou et al. 2004). It was shown that polarimetric X-band radars can be an effective tool for high temporal and spatial resolution rainfall parameter retrievals. The

Corresponding author address: Dr. Sergey Y. Matrosov, CIRES, University of Colorado, and NOAA/Environmental Technology Laboratory, 325 Broadway, R/ET7, Boulder, CO 80305.
E-mail: Sergey.Matrosov@noaa.gov

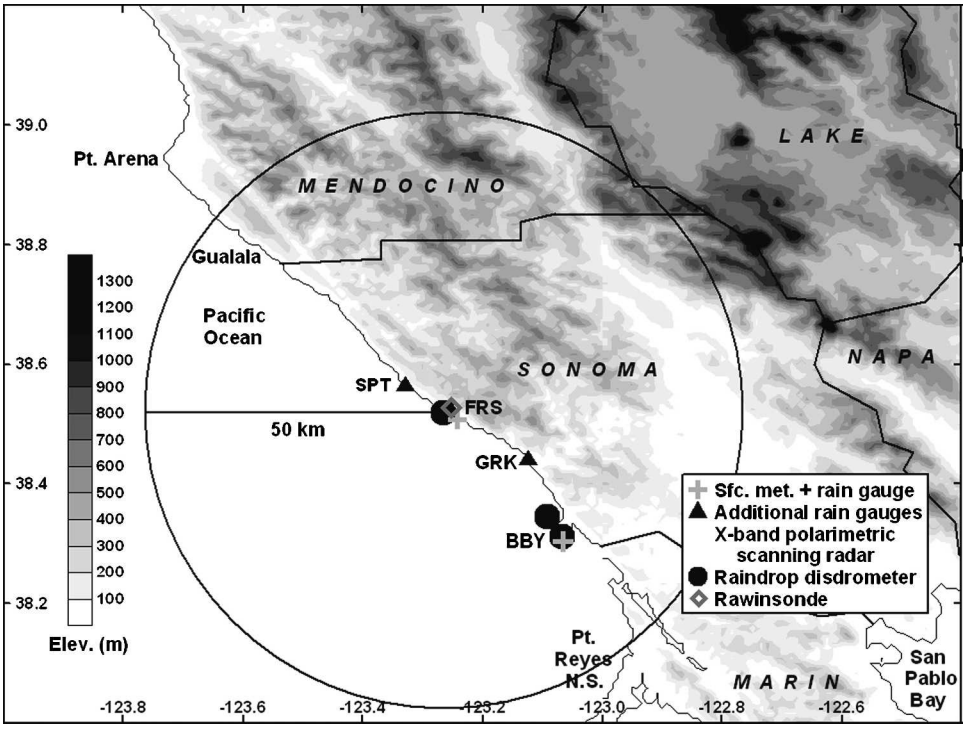

FIG. 1. The map of the HMT-04 research area showing locations of instruments mentioned in the text.

validations of X-band radar rainfall retrievals, however, were mostly performed using rain gauges and disdrometers that were located in a close proximity to the radar site (generally within a 12–15-km range). There still is a need to demonstrate the performance and to assess the effectiveness of X-band polarimetric radars for QPE measurements in a wider scope of meteorological conditions and at longer distances before the utility of these radars in different hydrometeorological applications and their use as gap fillers within the operational network coverage are fully realized.

Another important aspect of the utility of these radars is an assessment of how effective they can be for estimating parameters of drop size distributions (DSDs). While polarimetric X-band radars are somewhat disadvantaged in DSD parameter retrievals compared to S-band radars because of differential attenuation of differential reflectivity measurements, the effects of differential attenuation can be corrected in a manner similar to the reflectivity attenuation correction.

Some of these demonstration and assessment issues were addressed during the field deployment of the National Oceanic and Atmospheric Administration (NOAA) transportable polarimetric X-band radar during December 2003–March 2004 as part of the Hydrometeorological Testbed (HMT-04) project. This project was focused on improvements in QPE measurements and in hydrological forecast and warnings. The radar was deployed on the Pacific Ocean coastline at Fort Ross (FRS), California, near the mouth of the Russian River, in an area that has poor coverage by the NWS WSR-88Ds and is vulnerable to frequent flooding as a result of wintertime landfalling Pacific storms. Figure 1 shows a map of the research area. The radar had an almost unobstructed view of the ocean between the azimuthal directions of 120° and 310° and could observe approaching landfalling storms (a primary goal of the project), though the view inland at low radar elevation angles was blocked by the adjacent coastal mountains.

Technical characteristics of the NOAA/Environmental Technology Lab (ETL) X-band radar are given in Table 1 and, in more detail, by Martner et al. (2001). The scan sequences used for QPE were designed in 6-min cycles, which contained one low-elevation surveillance scan with 256 gates along the beam with a gate resolution of 225 m and a maximum range of 57.6 km. Each cycle also included five low-elevation (1° and 1.5°) "sea" scans with the 150-m gate resolution and a

TABLE 1. Main characteristics of the NOAA/ETL X-band radar.

Major capabilities: transportable, scanning, Doppler, polarimetric	
Frequency	9.34 GHz
Peak transmitted power	30 kW
Antenna	3.1-m diameter, 44-dB gain
Doppler processing	Pulse pair or time series
Platform	16-m flatbed trailer

TABLE 2. Dates, times, and accumulations (at FRS) of the winter rainstorms observed by the NOAA X-band radar during HMT-04 in the QPE measurement mode. Columns 3 and 4 show the percentage of the data points when polarimetric estimates of rainfall rate (for rains with $R > 0.1$ mm h^{-1}) and D_0 were available.

Storm period	Accumulation	Polarimetric R	Polarimetric D_0
1	2	3	4
0700 UTC 9 Dec–0000 UTC 10 Dec 2003	38.1 mm	29%	43%
0300 UTC 29 Dec–1300 UTC 29 Dec 2003	28.0 mm	23%	39%
0500 UTC 7 Jan–0800 UTC 7 Jan 2004	6.1 mm	26%	41%
1000 UTC 2 Feb–2000 UTC 2 Feb 2004	23.2 mm	31%	44%
1000 UTC 17 Feb–0700 UTC 18 Feb 2004	32.2 mm	14%	34%

maximum range of 38.4 km. Two range–height indicator (RHI) scans in each cycle were used to obtain the vertical structure of the observed storms. This scan strategy provided good coverage over the ocean and along the Sonoma County coast as well as offshore regions adjacent to the southern Mendocino and northern Marin County coasts (see Fig. 1).

Five significant landfalling storms were observed by the NOAA X-band radar during HMT-04 using the uninterrupted scan strategy mentioned above. These storms are listed in Table 2. Typical surface temperatures during these storms were 282–285 K, and the freezing level was located at altitudes of about 2–2.5 km above the ground. High-resolution (0.01 in.) tipping-bucket rain gauges used for validating rainfall retrievals were located at the Salt Point (SPT) State Park (the furthest unobstructed location northwest along the coast), Goat Rock (GRK), and Bodegy Bay (BBY) at the Bodega Bay Marine Laboratory of the University of California, Davis (see map in Fig. 1). These gauges recorded the number of 0.01-in. tips every 2 min. A Joss–Waldvogel impact disdrometer (JWD; Joss and Waldvogel 1967) was also deployed at the BBY site. It recorded DSDs every minute at the ground.

The NOAA X-band radar simultaneously transmits and simultaneously receives (STSR) horizontally and vertically polarized radar signals in the same measurement mode that has been recommended for polarimetric upgrades to the WSR-88Ds (Doviak et al. 2000). It allows measurements of all traditional radar polarization parameters such as differential phase shift, differential reflectivity, and correlation coefficient between horizontally and vertically polarized signals. Although depolarization ratio is valuable for identifying different hydrometeor types (e.g., Matrosov et al. 2001), this parameter is generally not readily available from polarimetric radars employing the STSR measurement mode. However, the NOAA-band radar does obtain circular depolarization ratio estimates using a special procedure (Matrosov 2004). Prior to its deployment in HMT-04, the vertically polarized measurements of the NOAA X-band radar were calibrated using a trihedral corner reflector (Martner et al. 2003). The horizontal polarization and differential reflectivity (Z_{DR}) calibrations were performed using observations of drizzle and the known vertical polarization calibration constants.

2. Correction of X-band radar signals for attenuation and differential attenuation

Attenuation of X-band radar signals in rain has been one of the main factors limiting the use of these radars for QPE purposes. Adding differential phase shift capability to X-band radars provides a relatively robust and a straightforward way to correct for the effects of partial attenuation in reflectivity. It has been shown (e.g., Bringi et al. 1990) that the specific differential phase shift in rain, K_{DP}, is practically linearly related to the specific attenuations (A_h or A_v) of radar reflectivities at linear horizontal (Z_{eh}) or vertical (Z_{ev}) polarizations and to the specific differential attenuation, A_{DP}, of Z_{DR}. Thus, the total two-way attenuation (ΔZ_{eh}) and differential attenuation (ΔZ_{DR}) corrections in rain consisting of nonspherical droplets can be expressed in terms of the total propagation differential phase shift, Φ_{DP}:

$$\Delta Z_{eh}(\text{dB}Z) = a_1 \Phi_{DP}(\text{deg}), \quad (1)$$

$$\Delta Z_{DR}(\text{dB}) = a_2 \Phi_{DP}(\text{deg}). \quad (2)$$

The coefficients a_1 and a_2 depend on the relation between the drop oblateness, which is characterized by the drop aspect ratio, r, and its equal-volume spherical diameter, D.

a. Examination of the coefficients a_1 and a_2

The linear model for the drop oblateness assumes the spherical shape for drizzle size drops ($D < 0.05$ cm) and a linear decrease of r with increasing D for larger drops:

$$r = (1. + 0.05b) - bD. \quad (3)$$

This model is a generalization of the linear model with a fixed value of $b = 0.62$ cm^{-1} that approximates data of Pruppacher and Beard (1970) and closely corresponds to the so-called equilibrium drop shape, which was until recently widely used for modeling in the polarimetric radar community. It was shown by Matrosov et al. (2002) that for a linear model (3), the coefficient a_1 at X band is almost inversely proportional to b, and a_2 is fairly independent of b. A number of later studies (e.g., Andsager et al. 1999; Brandes et al. 2004) indicated that drops are normally less oblate compared to

the equilibrium shape and r is generally not a linear function of D.

Examination of the function $r = f(D)$ from Brandes et al. (2004) shows, however, that this function is fairly linear and the majority of data points can be fitted by (3) with $b \approx 0.58$ cm^{-1}, if a few data points corresponding to unusually large drops ($D \geq 0.7$ cm) are ignored. Such large drops are rare, especially in wintertime stratiform rains. Indeed, modeling the A_h–K_{DP}, A_{DP}–K_{DP}, and R–K_{DP} relations at X band using the T-matrix approach for nonspherical drops (Barber and Yeh 1975) and JWD rain DSDs from HMT-04 with the drop shape (3), assuming $b = 0.58$ cm^{-1} and the polynomial fit of $r = f(D)$ from Brandes et al. (2004), generally results in differences of less than 12% in the coefficients of these relations. This modeling results in $a_1 \approx 0.25$ dB deg^{-1} and $a_2 \approx 0.033$ dB deg^{-1} (at 7°C), which is very close to the results obtained for similar values of b by Matrosov et al. (2002) based on the JWD DSDs collected on Wallops Island, Virginia.

Note that the use of experimental DSDs, rather than model gamma-function DSDs, helps to avoid some of the potential representativeness problems discussed by Illingworth and Blackman (2002). It is true even in light of some undercounts of small drops by JWD due to "dead" (i.e., recovery) time of the system after each drop impact. To mitigate the undercount issue, a dead-time correction was applied to the JWD DSD data as described by Sheppard and Joe (1994). For the HMT-04 dataset, accounting for the dead-time correction resulted in an average decrease of JWD-derived mass-weighted drop diameters by 3% and average increases of JWD-derived rainfall rates and reflectivities by about 9% and 5%, respectively.

There is currently no consensus in the radar meteorology community about the uniqueness of drop aspect ratio – size relations. In some rainfall retrieval techniques fixed relations are used (e.g., Brandes et al. 2004; Illingworth and Blackman 2002), while others treat b as an additional independent parameter (e.g., Gorgucci et al. 2001). Bringi et al. (2004) provide physical reasons for the variability in b. A combined polarimetric approach suggested by Matrosov et al. (2002) for X-band radar measurements also considers b as a variable and the corresponding estimator,

$$b \approx 12 Z_{eh}^{-0.36}(\text{mm}^6\ \text{m}^{-3}) K_{DP}^{0.40}(\text{deg km}^{-1}) Z_{dr}^{1.02}, \quad (4)$$

is similar to that of Gorgucci et al. (2000), after accounting for a general spectral dependence of K_{DP}. Note that Z_{dr} in (4) is in linear units: $Z_{DR}(\text{dB}) = 10 \log_{10}(Z_{dr})$.

Because of attenuation of Z_{eh} in rain, estimates of b at X band generally require an iteration procedure that corrects values of b at each iterative step. As a result, all rainfall estimators that use reflectivities corrected for attenuation are iterative in their nature. Figure 2a shows the probability distribution of the retrieved values of b based on applying (4) to the analyzed experimental dataset. The range and the azimuthal angle resolutions of the estimates are 150 m and 1°, respectively. The mean value of b is about 0.57 cm^{-1}. For a 1-dB error in Z_{eh}, a 0.3-dB error in Z_{DR}, and a 20% error in K_{DP}, the uncertainty of the retrievals of b due to the measurements errors is about 14%, assuming the independence of error contributions. This uncertainty can be as high as about 24% if, due to attenuation and differential attenuation corrections, errors in Z_{eh} and Z_{DR} double. One can also expect at least an 8%–10% uncertainty in in b retrievals due to variability in DSD details (Matrosov et al. 2002). Overall the uncertainty of b estimates is not much smaller than the standard deviation of the distribution in Fig. 2. Figure 2b shows the probability distribution of the values of b averaged along the radar beam (i.e., one beam-averaged value of b is prescribed to the whole beam). With approximately the same mean value (0.57 cm^{-1}), the distribution in Fig. 2b is noticeably narrower than that in Fig. 2a.

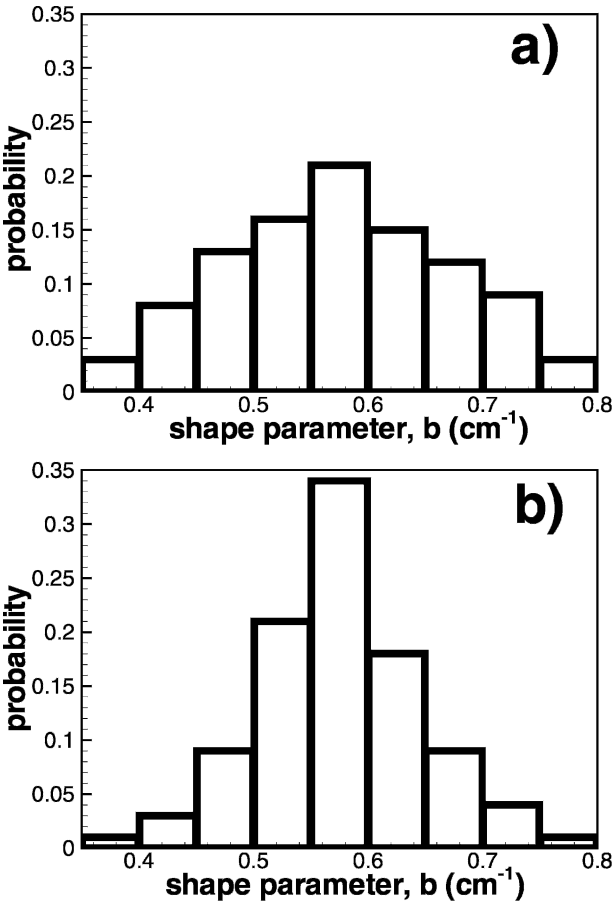

FIG. 2. Probability histograms of retrieved shape factor b for (a) 150-m resolution estimates and (b) mean values along the radar beam.

From the retrieval results in Fig. 2 and the previous discussion, it is reasonable to assume that values of b around 0.57–0.58 cm^{-1} describe average conditions

fairly well. Since the prospective goal of the ETL X-band radar operations is to produce near–real time polarimetric rainfall estimates, it is highly desirable to simplify the attenuation correction scheme for such operations. The use of the fixed value of $b \approx 0.57$ cm^{-1} and hence a fixed value of $a_1 \approx 0.25$ dB deg^{-1} for the attenuation correction makes the iterative procedure unnecessary, even if rainfall estimators still intrinsically account for changes of b in a given resolution volume when retrieving rainfall rates R. The use of different rainfall estimators, discussed in more detail in the next section, showed that applying the iterative attenuation correction scheme and the scheme that uses the fixed coefficient $a_1 \approx 0.25$ dB deg^{-1} results in differences in 1-h accumulations that typically do not exceed few percent for the HMT-04 dataset. This justifies using a simpler attenuation correction scheme for future near–real time retrievals.

Note that unlike a_1, a_2 is not very sensitive to b, so the differential attenuation correction of Z_{DR} measurements does not require iterations. It should be mentioned also that mean values $b \approx 0.57$ cm^{-1}, $a_1 \approx 0.25$ dB deg^{-1}, and $a_2 \approx 0.033$ dB deg^{-1} suggested here were found from DSD data collected during HMT-04 and are likely to be appropriate, on average, for winter storms on the coast of northern California but not necessarily for a broader range of rain conditions. There are indications (at least at C band) that a_1 and a_2 tend to increase when very large drops resulting in $Z_{DR} >$ 2–3 dB are present (Carey et al. 2000). However, as it will be illustrated in section 4, such large Z_{DR} values are uncommon in these storms. Case to case variabilities can be as high as $\Delta a_1 = 0.04$ dB deg^{-1} and $\Delta a_2 = 0.005$ dB deg^{-1}. Mean values of a_1 and a_2 correspond to a temperature of about 7°C. A 5°C variation in temperature can result in about 5% changes in these coefficients.

The attenuation/differential attenuation corrections in rain are calculated using (1) and (2) where the filtered values of the measured total differential phase shift, $\Phi_{DP}^{(m)}$, are used. The total phase shift at a given distance, d, is related to the propagation differential phase shift Φ_{DP} as

$$\Phi_{DP}^{(m)}(d) = \Phi_{DP}(d) + \delta(d), \quad (5)$$

where $\delta(d)$ is the backscatter phase shift. The backscatter phase shift contribution potentially can be recognized as a relatively abrupt increase (typically exceeding a standard deviation of Φ_{DP} measurements) followed by a decrease in an otherwise relatively monotonic trend of measured differential phase. Although no obvious manifestations of δ were evident in the HMT-04 data, suspicious spikes were filtered out in the process of smoothing differential phase shift data.

b. Possible unaccounted attenuation in rain

Very light rain does not produce clear trends of Φ_{DP} as a function of range because small raindrops are approximately spherical. The experience with the NOAA X-band radar rainfall measurements indicate that, on average, for rainfall rates less than about 2 mm h^{-1}, noise in $\Phi_{DP}^{(m)}$ data prevents reliable estimates of small total differential phase accumulations. Such rains, however, still cause attenuation of the radar signals. Figure 3 shows an A_h–R scatterplot calculated from DSDs collected by the JWD for a light-rain period on 17 February 2004. These results are typical for the HMT-04 dataset.

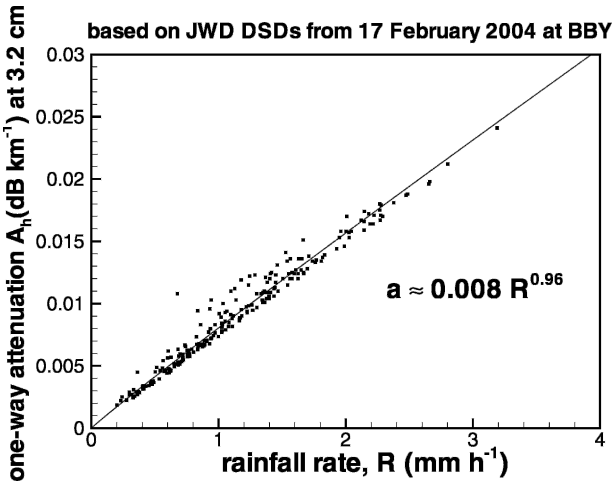

FIG. 3. Attenuation coefficient at X band vs rain rate for light rains.

It can be concluded, using the data in Fig. 3, that if rain with $R \approx 1$ mm h^{-1} fills a 40-km extent of the radar beam, the total two-way attenuation at distant ranges can be about 0.7 dB. This is somewhat smaller than the uncertainty of the radar absolute calibration, which is of the order of at least 1 dB. No special accounting for light-rain attenuation was made with the HMT-04 data, though in the future some reflectivity-based algorithms can be developed to account for this attenuation.

c. Attenuation of X-band radar signals in atmospheric gases

Gaseous attenuation of radar signals is almost universally neglected (except for cloud radars) though it can be appreciable at X band. Oxygen and water vapor are the main gaseous constituents that absorb radio signals causing attenuation. Absorption models discussed by Ulaby et al. (1981) were used to model two-way gaseous attenuation at the 3.2-cm wavelength of the NOAA/ETL X-band radar. Figure 4 shows the results of this modeling for 1° and 2° radar elevations and rain mean temperatures of 278 and 283 K. It was assumed that the relative humidity in the rain layer was RH = 90%.

It can be seen from Fig. 4 that the gaseous attenuation can be as high as 1 dB at 40-km range. This attenuation is relatively straightforward to correct since it

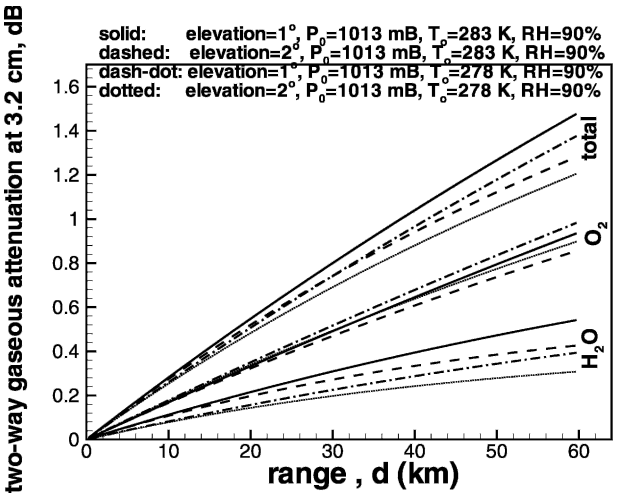

FIG. 4. Two-way gaseous attenuation at X band.

monotonically increases with range. The following simple approximations are suggested for two-way reflectivity corrections for gaseous attenuation at X band as a function of range, d, in kilometers:

$$\Delta Z_e^{(g)} \approx 0.030 d^{0.96} (\text{elevation 1 deg}). \quad (6)$$

These corrections are appropriate for typical conditions during HMT-04, and they were used in processing the NOAA X-band radar measurements.

d. Illustrations of the attenuation correction scheme

Figure 5 shows the (a) measured and (b) corrected values of Z_{eh} as observed by the radar from a 1.5° elevation scan over the ocean on 2 February 2004. Substantial attenuation effects are evident in the measured field. These effects are strongest behind an intense cell located at 10–12 km between the azimuthal directions 290° and 310°. The correction scheme described above works rather effectively, providing corrected reflectivities in near–real time. One obvious and important limitation of this (and any other) scheme is that nonattenuated radar reflectivities cannot be reconstructed when the measured signals are totally extinguished due to attenuation. The linear dynamic range of the NOAA X-band radar receivers is only about 50 dB (for comparison, the dynamic range of NEXRADs is about 90 dB). This is a limitation of the current radar whose dynamic range could be improved by 20 dB or more with hardware upgrades. It was estimated that during any given scan at the precipitation-scan-mode maximum range of 38.4 km, the relative area of the radar coverage where total extinction is achieved did not typically exceed 10%–15%. For most of the scans it was significantly less than that. Increasing the sensitivity and dynamic range of the radar will alleviate this limitation and allow QPE for longer ranges.

During HMT-04 operations, high cliffs at an azimuth

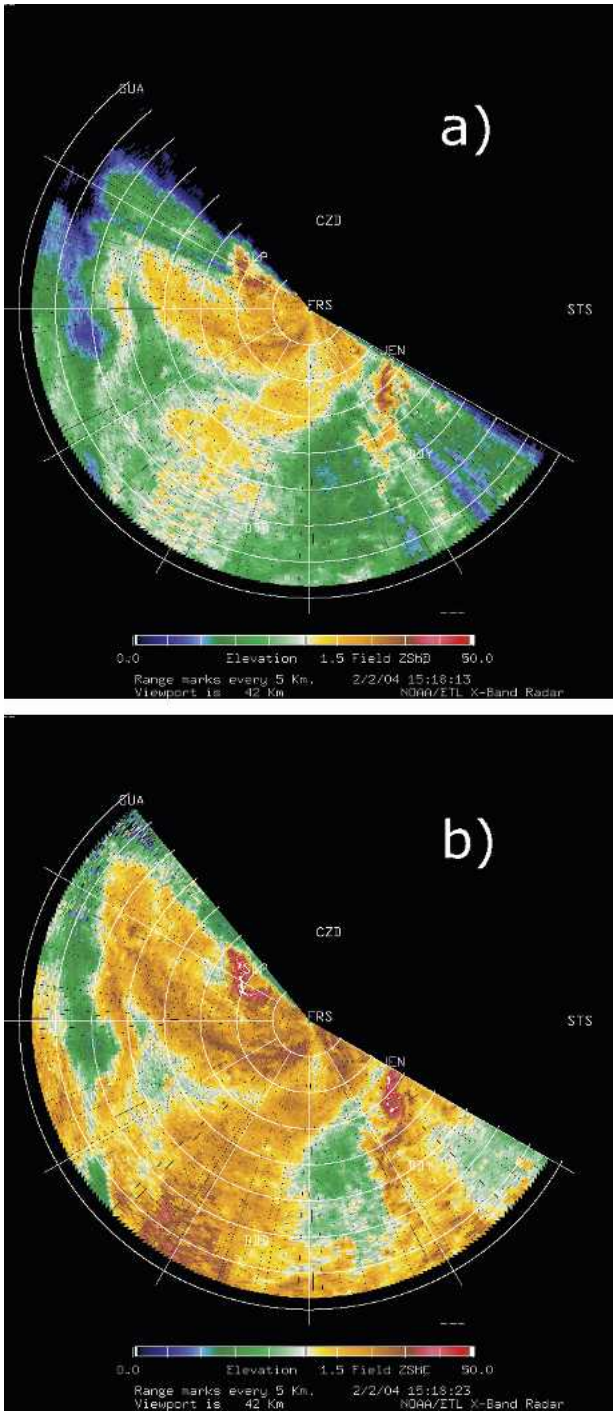

FIG. 5. Real-time NOAA X-band radar displays of (a) measured and (b) corrected for attenuation values of reflectivity on horizontal polarization, Z_h.

of 128.7° and 17.5-km range provided a useful, strong ground clutter target. Figure 6 shows (a) measured and (b) corrected reflectivities of the clutter point during the 1° elevation scans as a function of differential phase shift during one of the storms. Because of a beam align-

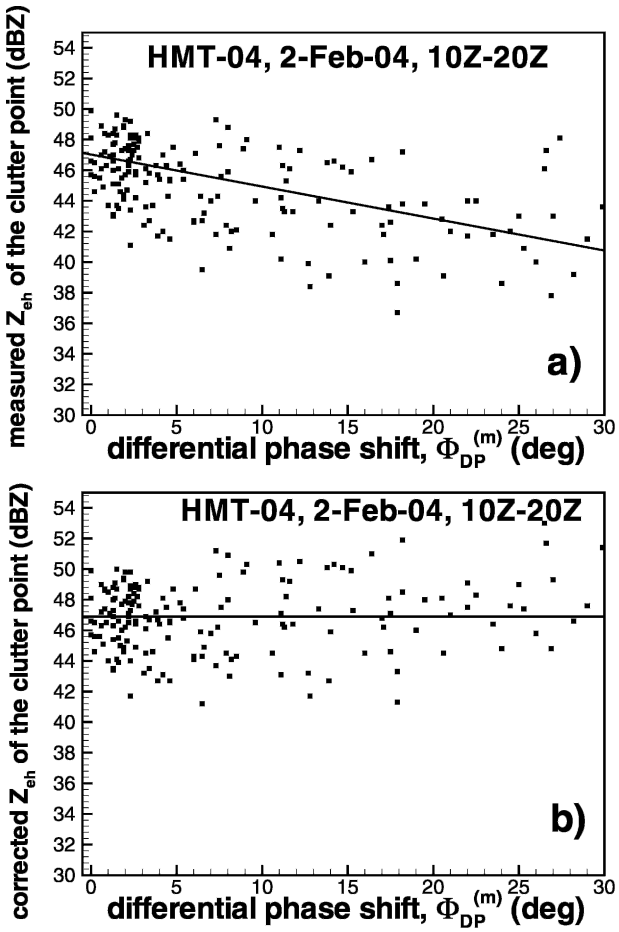

FIG. 6. (a) Measured and (b) corrected for attenuation values of reflectivity corresponding to a mountain clutter point pixel as a function of the measured differential phase shift between this point and the radar site.

ment uncertainty and a relatively high scan rate of 8 deg s^{-1}, the actual direction was almost never exactly 128.7° in azimuth and 1° in elevation, so the data in Fig. 6 correspond to the beam direction intervals of 128.3° < azimuth < 129.1° and 0.95° < elevation < 1.05°. Despite the uncertainty of the beam alignment and the associated variability in clutter reflectivity measurements, one can see a clearly decreasing trend in measured clutter reflectivities as a function of $\Phi_{DP}^{(m)}$ (Fig. 6a) and practically an absence of any noticeable trend in corrected reflectivity estimates (Fig. 6b). The decreasing trend in Fig. 6a is in accord with (1) when $a_1 \approx 0.25$ dB deg^{-1} (the gaseous attenuation is small at this range). These clutter measurement results independently indicate the general consistency of the attenuation correction scheme.

Another check of the performance of the attenuation and differential attenuation correction schemes is made by comparing measured and corrected radar reflectivities with calculations using the raindrop spectra observed in situ with the JWD with the shape factor $b = 0.57$ cm^{-1}. Figure 7 shows this comparison for a period of rain observed on 2 February 2004. Data points correspond to the times when the radar beam was approximately above the BBY site, which was located at 25 km in the azimuthal direction of 146°. Given vastly different sampling volumes of the radar and JWD, the height of the center of the radar beam above the ground level (AGL) of about 440 m, and the uncertainty in radar calibration, the agreement between corrected values of Z_{eh} and Z_{DR} with their calculation estimates from JWD DSDs can be considered quite good. The attenuation and differential attenuation corrections for the time period shown in Fig. 7 were frequently as large as 10 and 1.3 dB, respectively, and are about the largest encountered over BBY during HMT-04. Overall for the experiment, the relative biases for measured radar parameters above this site were −3.3 dB (for Z_{eh}) and 0.8 dB (for Z_{DR}) when rain was present. Applications of attenuation and differential attenuation corrections reduced these biases to 0.9 and

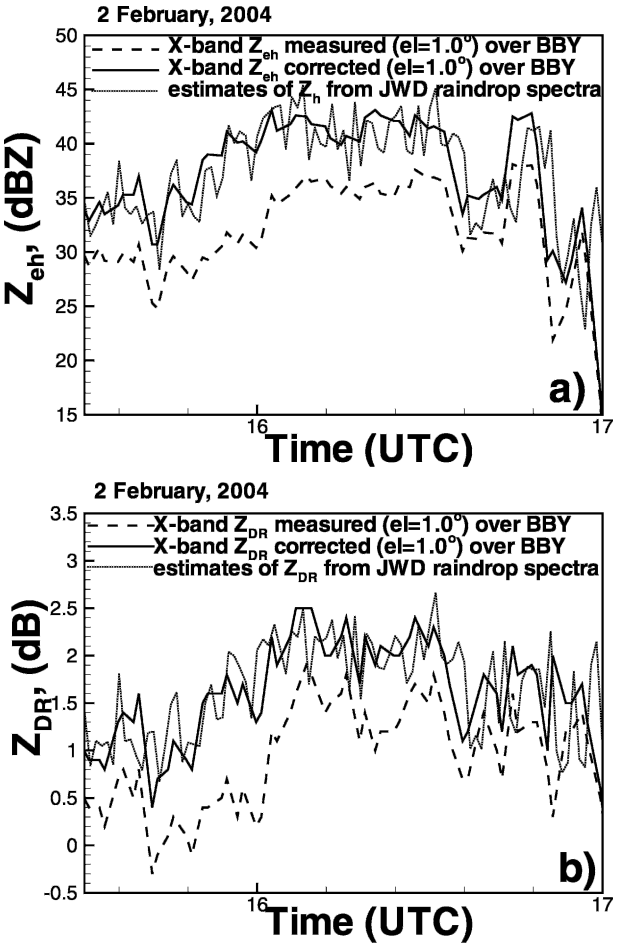

FIG. 7. Comparisons of radar (a) measured and corrected for attenuation reflectivities and (b) measured and corrected for differential attenuation differential reflectivities over the Bodega Bay site with estimates from the impact disdrometer.

−0.2 dB correspondingly, which is generally within typical uncertainties of radar measurements. When estimating these biases, an average time offset of 70 s between radar and JWD data was accounted for, and data, for which the attenuation correction was at least 1 dB, were considered. This time offset is seen from Fig. 7 where data calculated from JWD DSDs are generally lagging behind the X-band data, which is explained by the time it takes for the drops to fall from the radar sampling altitude to the ground.

Although these illustrations of the attenuation correction scheme performance cannot be regarded as a strict validation of this scheme, the presented results indicate a general consistency and robustness of the correction procedure. It provides confidence that the X-band radar reflectivity measurements can be effectively corrected for partial attenuation in real time. Some additional aspects of consistency for the differential attenuation correction procedure are discussed in more detail in section 4.

3. X-band estimates of instantaneous rainfall rates and accumulations

a. Rainfall rate estimators at X band

T-matrix modeling with DSDs collected by the JWD during HMT-04 resulted in the following mean K_{DP}–R relation for the average value of the shape parameter $b \approx 0.57$ cm^{-1}:

$$R(\text{mm h}^{-1}) \approx 14K_{DP}(\text{deg km}^{-1})^{0.8}. \quad (7)$$

This relation was derived assuming drop fall velocities at sea level. At the altitude of the center of the radar beam, h, these velocities are larger by a dimensionless factor:

$$c(h) = 1.1\rho(h)^{-0.45}, \quad (8)$$

where ρ (kg m^{-3}) is the air density at this height (Matrosov et al. 2002). In the HMT-04 polarimetric radar scanning mode, $c(h)$ did not exceed 1.03 at 1° beam elevation, and the velocity correction was neglected.

Relation (7) is very close to that obtained using the Wallops Island DSD dataset with a similar value of b (Matrosov et al. 2002). If one assumes the drop aspect ratio from Brandes et al. (2004), it will result in relatively minor changes in (7) that mostly affect the exponent (0.78 versus 0.82), while the coefficient does not change significantly.

The combined polarimetric estimator suggested by Matrosov et al. (2002) implicitly accounts for changes in the shape factor b in the resolution volume when making an estimate of instantaneous rainfall rate and shows only very modest sensitivity to the details of DSD:

$$R(\text{mm h}^{-1}) \approx 1.1Z_{eh}(\text{mm}^6\,\text{m}^{-3})^{0.3}K_{DP}(\text{deg km}^{-1})^{0.52} Z_{dr}^{-0.82}. \quad (9)$$

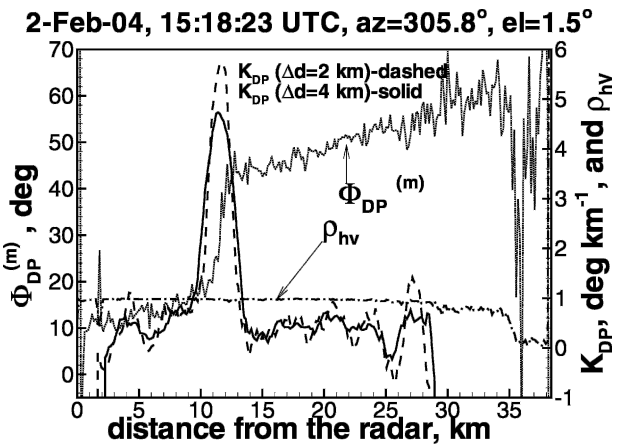

FIG. 8. An example of K_{DP} estimates along a radar beam in the presence of a heavy rain cell.

Model calculations with DSD spectra collected by the JWD in the analyzed observational cases observed during HMT-04 indicated also that the following X-band reflectivity-based relation described the experimental data in a mean sense:

$$Z_{eh}(\text{mm}^6\,\text{m}^{-3}) = 180R(\text{mm h}^{-1})^{1.4}. \quad (10)$$

In regular processing of the NOAA X-band radar data, the specific differential phase K_{DP} was estimated as a slope of the linear fit (i.e., the range derivative) to the differential phase shift measurements. Prior to estimating K_{DP}, the measured $\Phi_{DP}^{(m)}$ data were filtered for data quality. During the filtration process all data points with a low signal-to-noise ratio and with the copolar correlation coefficient $\rho_{hv} < 0.9$ were excluded. Also excluded were all spurious data points that were identified as spikes that exceeded three standard deviation values from a general $\Phi_{DP}^{(m)}$ trend. A 4-km sliding-window interval was typically used for K_{DP} estimates. At such relatively large intervals, some undesirable effects—such as the manifestations of nonuniform beam filling (Gosset 2004)—affecting K_{DP} estimates are minimized. Although smoothing to the K_{DP}-derived instantaneous rainfall fields is introduced through this procedure, it does not significantly affect the rain accumulation values. Figure 8 illustrates the effect of a sliding-window interval Δd on K_{DP} estimates. The data shown in this figure correspond to the beam penetrating the cell of heavy rain in the azimuthal direction of 305° (see Fig. 5). The maximum of K_{DP} for $\Delta d = 2$ km is larger and narrower compared to K_{DP} for $\Delta d = 4$ km. The total integral areas under both $K_{DP}(d)$ curves, however, are very similar, which results in approximately the same K_{DP}-based estimates of accumulation as the cell moves. Receiver output (not shown) indicates that radar echoes are in saturation for the first 1.5 km and they are practically extinct at ranges beyond about 29 km, which results in the absence of K_{DP} data there.

No obvious manifestations of the backscatter phase shift δ were noticed in the X-band data during HMT-04. One possible explanation for this is a gradual monotonic increase of δ as the drop size increases (and, hence, some cancellation of δ contributions when making K_{DP} estimates) and the lack of a strong δ "resonance" such as one at C band for large drops (Matrosov et al. 2002). Filtering differential phase shift data may also eliminate some possible δ contaminations.

Three different estimators of instantaneous rainfall rates were used for processing HMT-04 data: (a) the mean Z_{eh}–R relation (10), (b) the mean K_{DP}-based estimator (7), and (c) the combined polarimetric estimator (9). The values of Z_{eh} and Z_{dr} used in these estimators were corrected for the attenuation/differential attenuation effects as described in section 2. The estimates from the Z_{eh}–R relation were available in real time while the results from the other estimators were produced in postprocessing. The experience with processing the NOAA X-band polarimetric radar data from HMT-04 and from previous field experiments shows that K_{DP} estimates become very noisy for lower rainfall rates when the drops are nearly spherical and their polarimetric signatures are very weak. Because of high uncertainties of K_{DP} estimates at such conditions it was decided not to use polarimetric estimators (7) and (9) for HMT-04 data processing at the radar range gates for which either the corrected value of Z_{eh} was less than 27 dBZ or an estimate of K_{DP} was less than 0.1 deg km^{-1}. Both these conditions approximately correspond to rainfall rates around 2–2.5 mm h^{-1}. When at least one of these conditions was satisfied the rainfall rate from the mean Z_{eh}–R relation was used also in estimators (b) and (c) instead of Eqs. (7) and (9), respectively. Table 2 shows percentages of the rain data points where the polarimetric information was considered good enough to provide estimates of rainfall rates. No attempt was made to case-tune the Z_{eh}–R relation on an event-to-event basis because the DSD information was not known until after the observed event and, as a result, typically cannot be used in future near–real time algorithms.

Figure 9 shows an example of retrieved instantaneous rainfall rates R from different estimators above the BBY site during 2 February 2004 (same time period as in Fig. 7). Estimates of rainfall rates from the JWD data are also shown. It can be seen that "reflectivity only" estimates are strongly overestimating values of R indicating that the mean Z_{eh}–R was not appropriate for this particular case. Both polarimetric estimators (i.e., the combined polarimetric estimator and the K_{DP}-based estimator), on the other hand, provide generally good agreement with JWD data in spite of the uncertainties associated with vastly different sampling volumes. The standard deviations of polarimetric estimates with respect to the JWD are around 40%, and their average bias is about 0.8 mm h^{-1} (for rainfall rates with R $>$ 3 mm h^{-1} where polarimetric data are meaningful). The JWD estimates of R may themselves be somewhat biased low because the total rainfall accumulations for this case from JWD measurements were about 14% smaller than those inferred from the high-resolution rain gauge that was collocated with the JWD. The rainfall rate estimates from the gauge data are not shown because coarse temporal sampling of gauge tips (2 min) allows such estimates only in 7.6 mm h^{-1} increments.

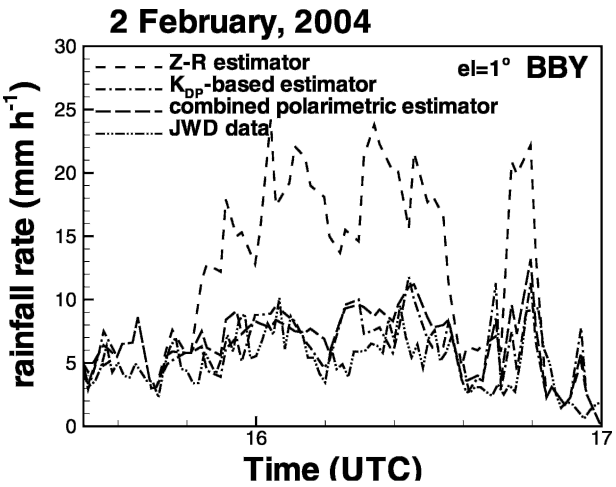

FIG. 9. An example of instantaneous rainfall retrievals over the Bodega Bay site.

The three discussed estimators for rainfall rate are straightforward and can be implemented to provide estimates in near–real time. It should be mentioned that other approaches also have been used in the past for estimating rainfall parameters from polarimetric X-band radar measurements. One of these approaches is the ZPHI method by Testud et al. (2000), which was adapted by Anagnostou et al. (2004). This method relies, in part, on a fixed power-law exponent in the correspondence between specific attenuation and reflectivity. DSDs from HMT-04 reveal, however, a significant scatter in this correspondence. Another factor that hampers the use of the ZPHI method with the HMT-04 dataset is the requirement for integration of the attenuated reflectivities along the radar beam for all the gates where rain is present. The limited dynamic range of the NOAA X-band radar often resulted in saturated signals at close ranges, so the attenuated reflectivity data were not available at these ranges.

b. Near–real time presentation of the data

Scan images of the X-band radar's measured reflectivity field from 1° elevation scans were posted on the Internet in near–real time every 6 min. Images of numerous other parameters, including attenuation-corrected reflectivity (such as in Fig. 5b), were available in real time at the radar and could also have been posted to the Internet. However, computations of the

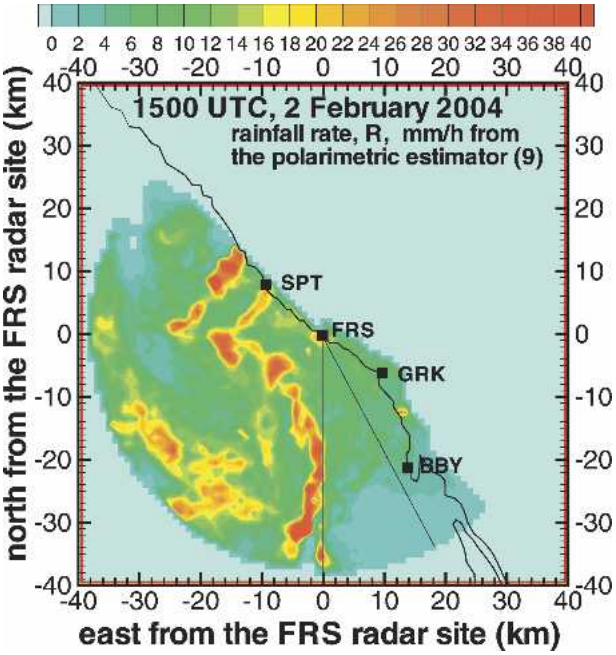

FIG. 10. An example of instantaneous rainfall rate retrievals from the combined polarimetric estimator at X band. The sector between the straight black lines at 150° and 180° was partially blocked by the radar trailer.

K_{DP}-based and combined polarimetric estimates of rainfall rate were conducted for HMT-04 in postprocessing, because these procedures were under development. In future deployments of the radar, it is feasible and desirable to compute these rainfall rates and storm-total rain accumulations in near–real time and to provide maps of them on the Internet as aids to weather and hydrological forecasters.

An example of instantaneous rainfall rate information is shown in Fig. 10. These data were obtained using the combined polarimetric estimator (9) for 1500 UTC on 2 February 2004. The retrievals were converted to a 1-km-resolution Cartesian grid centered at the radar location at FRS. The presentation of the results in the Cartesian grid provides the constant spatial resolution of the estimates, regardless of the distance from the radar. At the same time it retains the important spatial features of the measured rainfall field such as a line of strong showers with R reaching 40 mm h^{-1} and extending approximately in the north–south direction.

c. Estimations of rainfall accumulations

Rainfall accumulations for given time intervals and over the entire course of a storm present very important hydrological information. The radar-derived accumulations were obtained by time integrating the estimates of instantaneous rainfall rate. The accumulations were then compared to the three high-resolution (0.01 in.) tipping-bucket gauges that were deployed on the coast at the BBY (d = 24.8 km, azimuth = 146.2°), GRK(d = 11.3 km, azimuth = 126.3°), and SPT sites (d = 11.2 km, azimuth = 308.8°). Figure 11 shows two characteristic examples of these comparisons for the 2 February 2004 event at the GRK site and for the 17–18 February 2004 event at the BBY site. The rainfall accumulations for the different radar estimators above the gauge locations and for the gauge data at the ground are shown.

It can be seen that the mean Z_{eh}–R estimator significantly overestimates storm totals for the 2 February 2004 event, while both polarimetric estimators provide very close agreement with the gauge data. For the 17–18 February 2004 event, results from all three estimators are quite close, and results from all of them are between estimates from the gauge and the JWD that was collocated with the gauge. A difference of about 10% between the gauge and JWD accumulations for this event was the greatest of all analyzed rain events from HMT-04, though a difference of a few percent was

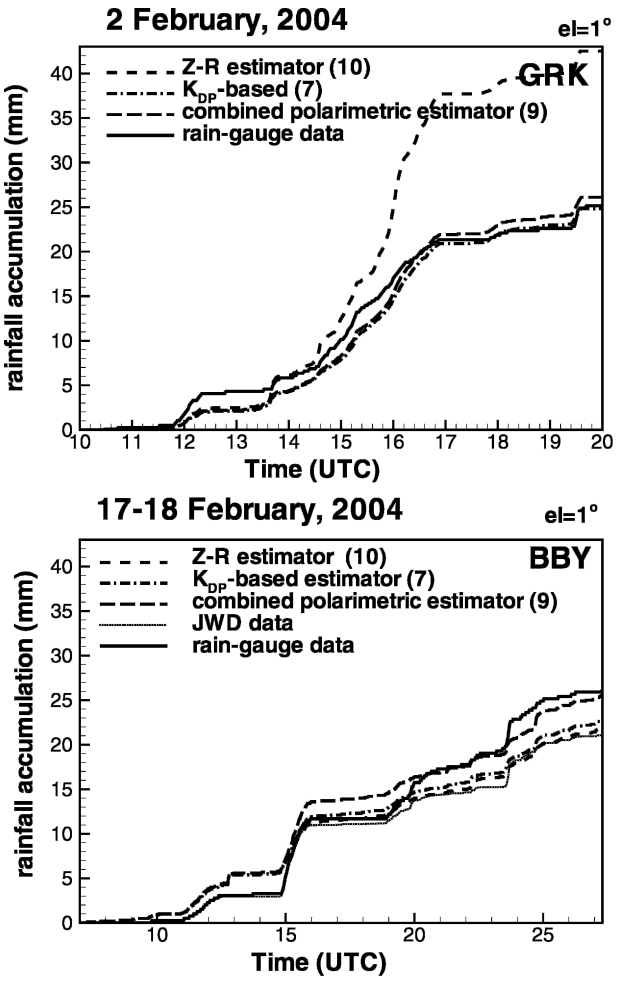

FIG. 11. Radar and gauge rainfall accumulations as a function of time for (a) the GRK site on 2 Feb 2004 and (b) the BBY site on 17–18 Feb 2004.

typical. The underestimation of the accumulation by JWD could be in part due to undercounting of small drops by the disdrometer (even after the dead-time correction), though this issue needs more detailed research, which is outside the scope of this study. The rain gauges used in this research were calibrated to an accuracy of about 5%, and hence the gauge data were considered as the accumulation "ground truth."

Some of the differences in gauge and radar-derived accumulations can be attributed to sampling volume issues and vertical variability in rainfall profiles. The center of the radar beam at 1° elevation was located at altitudes of about 440 and 200 m above the ground for the BBY and GRK sites, respectively. In fact, it was established from occasional RHI scans in the direction of the BBY site that rain at this site at around 1200 UTC on 2 February 2004 was mostly limited to a within few hundred meters above the ground. The radar beam during 1° elevation scans was mostly overshooting this shallow rain, which resulted in the lower radar estimates of accumulation during this time. Though such geometrical issues and the rain variability in between consecutive radar scans are valid issues in explaining some of the radar–gauge differences, the differences attributable to the uncertainty of radar-derived rainfall rates are the main interest in this study.

Comparing the total accumulations derived from the NOAA X-band radar data with those from the available gauges for the analyzed events that were observed during HMT-04 from December 2003 to February 2004 shows that the combined polarimetric estimator (9) provided, on average, the best results. The standard deviation between gauge data and accumulations from this estimator was 24%. The accumulations from the mean K_{DP}-based estimator (10) showed a standard deviation of 26%, and the accumulations obtained using the mean Z_{eh}–R relation were on average the least accurate, with standard deviations from the gauge estimations of 36%. The biases between the gauge accumulations and the radar-inferred data for all estimators were generally within 10%. These results are consistent with those found by Matrosov et al. (2002) at shorter ranges during the previous field campaign in Wallops Island, Virginia.

Since accumulation contributions of rainfall with $R >$ 3 mm h^{-1} are usually significant, there is a noticeable improvement in accumulation estimates, on average, if polarimetric measurements are used. Although the polarimetric estimators are not generally applicable for rain rates less than about 2–2.5 mm h^{-1}, they are nevertheless useful for estimating storm total accumulations, because often these accumulations were dominated by periods of heavier rain.

As previously mentioned, the accumulation information for HMT-04 was generated in postprocessing. As an example, Fig. 12 depicts the total 10-h rainfall accumulation for the storm of 2 February 2004 obtained using the time integration of the combined polarimetric estimate (9). There are no obvious trends in accumulation values as function of range, which indicates that the problems, associated with the "lost" rainfall due to total signal extinction, were not significant. The wedges of low accumulation values between the azimuthal directions of 150° and 180° are artifacts caused by the partial blockage of the radar beam by the top of the radar trailer. Estimates of storm accumulation from a nearby NEXRAD (KMUX) were as much as a factor of 5 lower than actually observed for this event, which was mainly attributed to the much higher altitude of NEXRAD scans (compared to the X-band scans) over the HMT-04 area. The accumulation values in Fig. 12 (as rainfall rates in Fig. 11) are presented in the Cartesian grid. The information of the type shown in Figs. 11 and 12 can be a valuable asset in weather nowcasting and for issuing warnings in the flood-prone areas or in providing uniquely high resolution QPE information for hydrologic models.

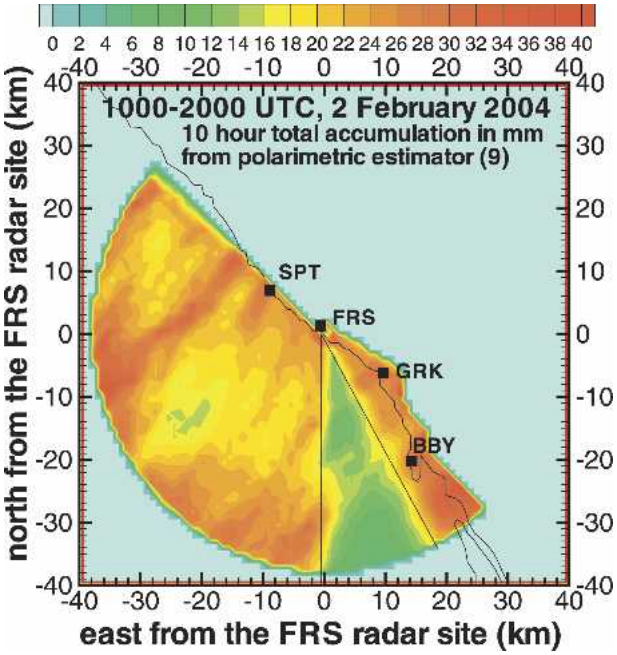

FIG. 12. A map of the total rainfall accumulation for the 2 Feb 2004 event obtained from X-band radar data. The sector between the straight black lines at 150° and 180° was partially blocked by the radar trailer.

4. Estimates of characteristic raindrop size from X-band radar measurements

Information on rainfall DSDs is very useful for many practical applications ranging from developing radar algorithms for spaceborne applications to distinguishing among different types of rain [e.g., as indicated by White et al. (2003), nonbrightband wintertime rains on the West Coast tend to consist of smaller drops com-

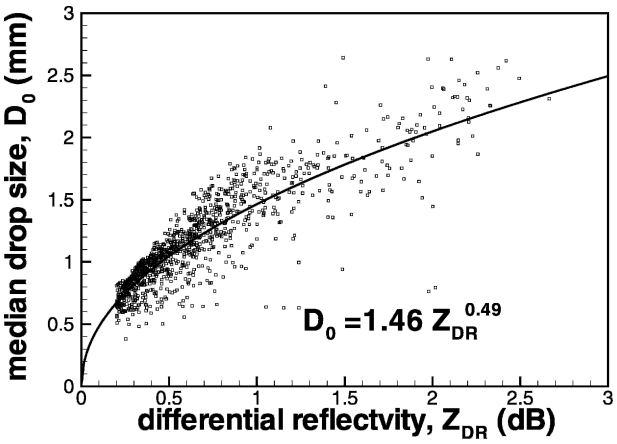

FIG. 13. A scatterplot between median drop size D_0 and differential reflectivity Z_{DR} at X band as modeled using DSDs from HMT-04.

pared to the stratiform brightband rains]. In their classic work, Seliga and Bringi (1976) suggested an approach to determine a drop size parameter that characterizes the whole DSD such as median diameter of the equal volume sphere D_0 from measurements of differential reflectivity Z_{DR}. This approach has subsequently been widely used in the radar meteorology community in different applications that primarily utilized longer wavelength radars. The main factor hampering its use for X-band radars was the problem of noticeable differential attenuation that corrupted Z_{DR} signals. The differential attenuation correction scheme described in section 2 provides a way to overcome this problem. DSD spectra collected with the use of the JWD at the Bodega Bay site also provide an opportunity to evaluate the robustness of D_0 estimates from the X-band Z_{DR} measurements, and, in a way, to assess the consistency of the differential attenuation corrections. In the field, Z_{DR} values were regularly calibrated using the radar's vertical beam measurements and also low-elevation-angle measurements in drizzle at close ranges.

Figure 13 shows a scatterplot between D_0 and Z_{DR} at X band calculated using the T-matrix method from DSD spectra that were measured by the JWD during HMT-04. Data interpolation was needed between the resolution bins of the JWD to obtain estimates of D_0 from measured spectra. The drop shape described by (3) was assumed with $b = 0.57\ \text{cm}^{-1}$. The best-fit power law is

$$D_0(\text{mm}) = 1.46 Z_{DR}^{0.49}(\text{dB}). \tag{11}$$

Changes in the assumption of b by $0.05\ \text{cm}^{-1}$ and the use of the drop shapes from Brandes et al. (2004) result in only about 6% changes in the coefficient in (11) which is negligible compared to the data scatter in Fig. 11. Given this and the fact that $b = 0.57\ \text{cm}^{-1}$ was estimated as the mean observed value, (11) can be considered appropriate for estimating median drop size in the HMT-04 storms. Because of the data scatter exhibited in Fig. 11 and a few tenths of 1-dB uncertainties in Z_{DR} measurements, estimates of D_0 at close ranges can have retrieval errors as large as about 0.3–0.4 mm. The retrieval errors will likely increase with range as additional uncertainties due to differential attenuation correction become more significant.

Closely related to D_0 is the mass-weighted mean diameter of the equal volume sphere D_m, which is another characteristic size describing the DSD:

$$D_m = \langle D^4 \rangle / \langle D^3 \rangle, \tag{12}$$

where the angular brackets mean averaging with respect to DSD. Some researchers prefer D_m over D_0 because calculations of D_m from experimental DSDs do not involve data interpolation between different bins of the JWD data; D_m is generally only slightly larger than D_0, and for the model gamma-function DSDs,

$$D_m D_0^{-1} = (\mu + 4)(\mu + 3.67)^{-1}. \tag{13}$$

The use of DSDs from HMT-04 with the same assumptions that were made when deriving (11) results in

$$D_m(\text{mm}) = 1.63 Z_{DR}^{0.48}(\text{dB}). \tag{14}$$

Note that (11) and (14) are consistent with (13) for small values of μ.

Figure 14 shows examples of comparisons of median drop sizes retrieved from X-band differential reflectivity measurements using (11) and estimates from JWD DSDs for the times when the radar beam passed over the BBY site at 1° elevation (i.e., about 440 m AGL). No attempts were made to retrieve D_0 from the radar data when the corrected Z_{DR} values were less than 0.25 dB, which approximately corresponds to the noise level of differential reflectivity measurements and results in $D_0 \approx 0.75$ mm when using the estimator (11). The percentage of rain data points that satisfied the 0.25-dB threshold is shown in Table 2. This percentage is typically greater than that when the polarimetric information was used to retrieve rainfall rates because K_{DP} data were often still too noisy while Z_{DR} values were considered good.

It can be seen that the agreement between JWD and radar estimates of D_0 are quite good for most of the comparison periods, especially during the time of heavier rain between 1500 and 1700 UTC on 2 February 2004. During some shorter periods (e.g., around 1900 UTC on 2 February), however, the radar failed to detect drops with D_0 exceeding 1 mm. In part this could be due (but not necessarily) to the differences in sampling volumes and vertical variability of characteristic drop sizes between the ground level and aloft. The standard deviations of radar-derived values of D_0 relative to the JWD data (for data points where radar retrievals are available, and after accounting for the time re-

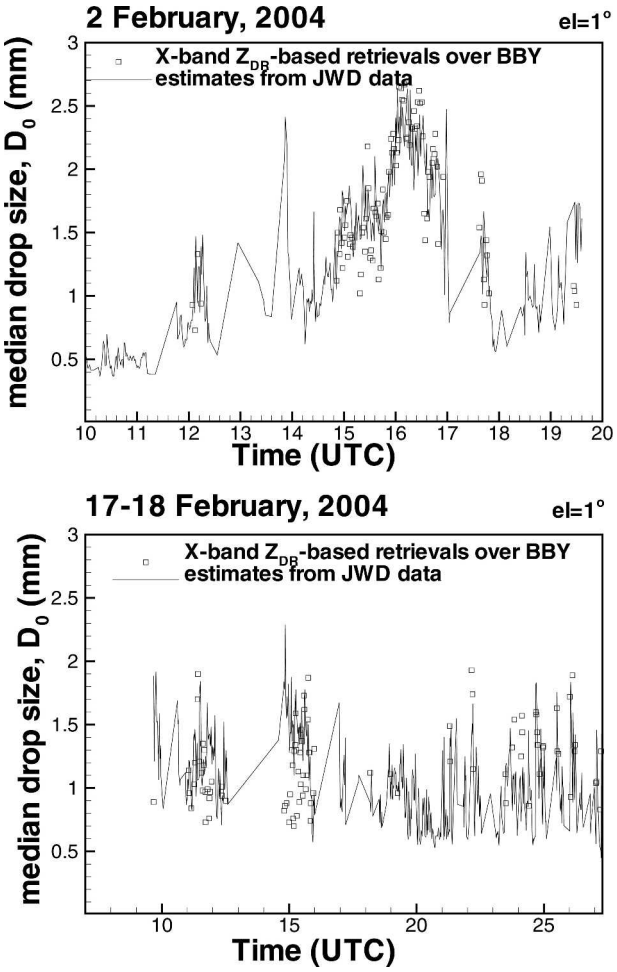

FIG. 14. Comparisons of radar retrievals of D_0 with estimates from DSDs measured by the disdrometer for (a) 2 Feb 2004 and (b) 17–18 Feb 2004.

quired for drops to reach the ground from the radar sampling altitude) are about 0.22 mm for the 2 February case (Fig. 14a) and about 0.28 mm for the 17–18 February case. Possible undersampling of small drops (even after the dead-time correction) might affect the JWD estimates of drop sizes, though the biases related to this undersampling are expected to be much smaller than the standard deviations mentioned above. Results shown here are quite representative of the other analyzed cases from HMT-04.

Overall good agreement between radar-derived and in situ estimates of D_0 indicates the general robustness of the differential attenuation correction scheme described earlier and used to correct differential reflectivity values prior to their use in the estimator (11). Especially encouraging is the fact that good agreement between radar and in situ estimates of D_0 was reached at relatively large distances from the radar (compared to the Wallops Island work) where differential reflectivity corrections were substantial.

These comparison results indicate that X-band polarimetric radars can be successfully used for drop size distribution retrievals at moderately long ranges. This demonstrates the promise for using X-band radars to obtain reasonably accurate drop size characteristics in a manner similar to that used with longer-wavelength radars (such as those at S band) that do not experience much differential attenuation. No attempts have yet been made to retrieve another important parameter describing the DSD shape (i.e., μ, the order of the assumed gamma-function DSD) from X-band radar measurements. Brandes et al. (2004), however, suggest that there is a strong correlation between the slope of the gamma function DSD, Λ, and μ. If this is true, there should also be a strong correlation between D_0 and μ because

$$\Lambda = (3.67 + \mu)D_0^{-1}. \tag{15}$$

In this case, independent estimations of μ might not be necessary.

5. Conclusions

The experience gained with using the NOAA X-band transportable polarimetric radar in different recent field campaigns showed that this radar is capable of providing high-resolution and accurate estimates of rainfall parameters. Polarimetric schemes that use differential phase shift measurements allow for an efficient correction for the partial attenuation and differential attenuation effects in rain, thus overcoming these major limitation factors that have precluded the wider use of X-band radar for QPE in the past. An additional correction for the gaseous attenuation of X-band signals was suggested in this study. Different verification procedures (e.g., comparisons of attenuated and nonattenuated measurements of ground clutter and comparisons between measured and corrected radar reflectivities and corresponding estimates from JWD DSDs) indicate a general robustness of the attenuation correction scheme devised for a mean raindrop shape factor $b \approx 0.57$ cm^{-1}. The iterative correction procedure, which accounts for local variabilities of the shape factor, changes final QPE results only slightly and thus can be avoided if there is a priority in providing quick near–real time estimates.

During the HMT-04 field project, the NOAA X-band radar, with its noise level of about -100 dBM and a modest linear receiver dynamic range of about 50 dB, was able to effectively provide QPE with high temporal resolution (1 min) within the range of about 40 km from the radar with occasional surveillance scans with the maximum range close to 60 km. During the routine scans with the maximum range set at about 40 km, areas of the total signal extinction, with no possibility of recovering radar signals due to heavy attenuation, were quite limited, and this did not significantly diminish the

performance of the radar. Improving the noise level of the radar receivers, increasing the transmitter power and raising the dynamic range of the receivers can further increase the usable range coverage for QPE. All of these engineering improvements are feasible and desirable.

Three different estimators were used to calculate rainfall rates from the X-band radar measurements during a 3-month deployment in HMT-04. Based on comparisons with the total accumulations recorded by the high-resolution rain gauges located along the coast, it was shown that the use of the mean Z_{eh}–R relation (where Z_{eh} is the horizontal polarization reflectivity corrected for attenuation) devised for this area can result in 36% of uncertainty in accumulation estimates. The use of the mean K_{DP}–R relation in areas of good differential phase measurements instead of the mean Z_{eh}–R relation decreases the uncertainty of accumulation estimates to 26%. An additional inclusion of Z_{DR} measurements in the combined polarimetric estimator further reduces uncertainty to 24%. The combined polarimetric estimator intrinsically accounts for the raindrop shape factor changes in the radar resolution volume, while the attenuation correction scheme uses the mean drop shape to avoid an iterative procedure for retrievals. The demonstrated agreement between the polarimetric X-band radar and gauge accumulations should be considered quite satisfactory, given potential gauge errors and uncertainties associated with vastly different scales of radar and gauge measurements (Ciach and Krajewski 1999; Steiner and Smith 2004). A more thorough assessment of X-band radar QPE over a denser network of rain gauges that are located further distances (greater than 25–30 km) is certainly desirable. However, the results shown here indicate that X-band approaches have definite promise and application potential.

It was also demonstrated that differential reflectivity measurements corrected for differential attenuation effects can be efficiently used for estimating characteristic sizes of raindrops such as median volume diameters. The radar-derived characteristic sizes compared well with those from impact disdrometer estimates. If an assumption about gamma-function size distributions is made, distribution parameters other than median drop size can also be potentially estimated either through additional polarimetric measurements or using the intrinsic correlation between D_0 and the order of gamma distribution μ.

The use of the NOAA X-band radar during HMT-04 showed that it can provide accurate estimates of rainfall accumulations in the important area that is prone to flooding during wintertime landfalling Pacific storms. This area of the Sonoma County and south Mendocino County coast lacks adequate coverage by the weather network WSR-88Ds (e.g., Westrick et al. 1999), and data from these radars can result in large underestimations of rainfall accumulations. Though a comprehensive study of deficiencies in WSR-88D estimates in this area is beyond the scope of the current work, initial estimates show that the total storm accumulations from NEXRADs in this area can be a factor of 5 or so too low in the case of shallow storms. It is intended that in future field projects the NOAA X-band radar will provide near–real time information on rainfall parameters through the Internet.

Acknowledgments. Authors are thankful to Kurt Clark, Allen White, Thomas Ayres, Paul Neiman, David White, Irina Djalalova, Clark King, and Scott Abbot, who actively took part in the HMT-04 field project. The Fort Ross site for the X-band radar was provided by the California Department of Parks and Recreation.

REFERENCES

Anagnostou, E. N., M. N. Anagnostou, W. F. Krajewski, A. Kruger, and B. J. Miriovsky, 2004: High resolution rainfall estimation from X-band polarimetric radar measurements. *J. Hydrometeor.,* **5,** 110–128.

Andsager, K., K. V. Beard, and N. F. Laird, 1999: Laboratory measurements of axis ratios for large raindrops. *J. Atmos. Sci.,* **56,** 2673–2683.

Barber, P., and C. Yeh, 1975: Scattering of electromagnetic waves by arbitrarily shaped dielectric bodies. *Appl. Opt.,* **14,** 2864–2872.

Brandes, E. A., G. Zhang, and J. Vivekanandan, 2004: Comparison of polarimetric radar drop size distribution retrieval algorithms. *J. Atmos. Oceanic Technol.,* **21,** 584–598.

Bringi, V. N., V. Chandrasekar, N. Balakrishnan, and D. S. Zrnic, 1990: An examination of propagation effects on radar measurements at microwave frequencies. *J. Atmos. Oceanic Technol.,* **7,** 829–840.

——, T. Tang, and V. Chandrasekar, 2004: Evaluation of a new polarimetrically based *Z*–*R* relation. *J. Atmos. Oceanic Technol.,* **21,** 612–623.

Carey, L. D., S. A. Rutledge, D. A. Ahijevich, and T. D. Keenan, 2000: Correcting propagation effects in C-band polarimetric radar observations of tropical convection using differential propagation phase. *J. Appl. Meteor.,* **39,** 1405–1433.

Ciach, G. J., and W. F. Krajewski, 1999: Radar–rain gauge comparisons under observational uncertainties. *J. Appl. Meteor.,* **38,** 1519–1525.

Doviak, R. J., V. Bringi, A. V. Ryzhkov, A. Zahrai, and D. Zrnic, 2000: Considerations for polarimetric upgrades to operational WSR-88D radars. *J. Atmos. Oceanic Technol.,* **17,** 257–278.

Gorgucci, E., G. Scarchilli, V. Chandrasekar, and V. N. Bringi, 2000: Measurement of mean raindrop shape from polarimetric radar observations. *J. Atmos. Sci.,* **57,** 3406–3413.

——, ——, ——, and ——, 2001: Rainfall estimation from polarimetric radar measurements: Composite algorithms immune to variability in raindrop shape–size relation. *J. Atmos. Oceanic Technol.,* **18,** 1773–1786.

Gosset, M., 2004: Effect of nonuniform beam filling on the propagation of radar signals at X-band frequences: Part II: Examination of differential phase shift. *J. Atmos. Oceanic Technol.,* **21,** 358–367.

Illingworth, A. J., and T. M. Blackman, 2002: The need to represent raindrop size spectra as normalized gamma distributions for the interpretation of polarization radar observations. *J. Appl. Meteor.,* **41,** 286–297.

Iwanami, K., R. Misumi, M. Maki, T. Wakayama, K. Hata, and S. Watanabe, 2001: Development of a multiparameter radar

system on mobile platform. Preprints, *30th Int. Conf. on Radar Meteorology*, Munich, Germany, Amer. Meteor. Soc., 104–106.

Joss, J., and A. Waldvogel, 1967: Ein Spektrograph für Niederschlagstropfen mit automatischer Auswertung. *Pure Appl. Geophys.,* **68,** 240–246.

Martner, B. E., K. A. Clark, S. Y. Matrosov, W. C. Campbell, and J. S. Gibson, 2001: NOAA/ETL's polarization-upgraded X-band "hydro" radar. Preprints, *30th Int. Conf. on Radar Meteorology*, Munich, Germany, Amer. Meteor. Soc., 101–103.

——, ——, and B. W. Bartram, 2003: Radar calibration using a trihedral corner reflector. Preprints, *31st Int. Conf. on Radar Meteorology*, Seattle, WA, Amer. Meteor. Soc., 1028–1030.

Matrosov, S. Y., 2004: Depolarization estimates from linear H and V measurements with weather radars operating in simultaneous transmission–simultaneous receiving mode. *J. Atmos. Oceanic Technol.,* **21,** 574–583.

——, R. A. Kropfli, R. F. Reinking, and B. E. Martner, 1999: Prospects for measuring rainfall using propagation differential phase in X and Ka-radar bands. *J. Appl. Meteor.,* **38,** 766–776.

——, R. F. Reinking, R. A. Kropfli, B. E. Martner, and B. W. Bartram, 2001: On the use of radar depolarization ratios for estimating shapes of ice hydrometeors in winter clouds. *J. Appl. Meteor.,* **40,** 479–490.

——, K. A. Clark, B. E. Martner, and A. Tokay, 2002: X-band polarimetric radar measurements of rainfall. *J. Appl. Meteor.,* **41,** 941–952.

National Research Council, 2004: *Flash Flood Forecasting over Complex Terrain: With an Assessment of the Sulphur Mountain NEXRAD in Southern California*. National Academy Press, 158 pp.

Pruppacher, H. R., and K. V. Beard, 1970: A wind tunnel investigation of the internal circulation and shape of water drops falling at terminal velocity in air. *Quart. J. Roy. Meteor. Soc.,* **96,** 247–256.

Seliga, T. A., and V. N. Bringi, 1976: Potential use of radar differential reflectivity measurements at orthogonal polarizations for measuring precipitation. *J. Appl. Meteor.,* **15,** 69–76.

Sheppard, B. E., and P. I. Joe, 1994: Comparisons of raindrop size distribution measurements by a Joss–Waldvogel disdrometer, a PMS 2DG spectrometer, and a POSS Doppler radar. *J. Atmos. Oceanic Technol.,* **11,** 874–887.

Steiner, M., and J. A. Smith, 2004: Scale dependence of radar rainfall rates—An assessment based on raindrop spectra. *J. Hydrometeor.,* **5,** 1171–1180.

Testud, J., E. Le Bouar, E. Obligis, and M. Ali-Mehenni, 2000: The rain profiling algorithm applied to polarimetric weather radar. *J. Atmos. Oceanic Technol.,* **17,** 332–356.

Ulaby, F. T., R. K. Moore, and A. K. Fung, 1981: *Fundamentals and Radiometry.* Vol. 1, *Microwave Remote Sensing: Active and Passive*, Addison-Wesley, 450 pp.

Westrick, K. J., C. F. Mass, and B. A. Colle, 1999: The limitations of the WSR-88D radar network for quantitative precipitation measurement over the coastal western United States. *Bull. Amer. Meteor. Soc.,* **80,** 2289–2298.

White, A. B., P. J. Neiman, F. M. Ralph, D. E. Kingsmill, and P. O. G. Persson, 2003: Coastal orographic rainfall processes observed by radar during the California Land-Falling Jets Experiment. *J. Hydrometeor.,* **4,** 264–282.

Wurman, J., 2001: The DOW mobile multiple Doppler network. Preprints, *30th Int. Conf. on Radar Meteorology*, Munich, Germany, Amer. Meteor. Soc., 95–97.